A Virtual HF Signal Injection Based Maximum Efficiency per Ampere Tracking Control for IPMSM Drive

Mengdi Li, Sheng Huang, Xuan Wu, Kan Liu, *Senior Member, IEEE*, Xiaoyan Peng, and Ge Liang

***Abstract*—In this article, a virtual high-frequency signal injection based searching method is proposed to derive the optimal current angle for the maximum efficiency per ampere control of interior permanent magnet synchronous machine (IPMSM) drive system. It injects a small virtual square wave HF signal into the mathematical model of IPMSM drive system including both the electrical machine and inverter, by which the optimal current angle could be accurately derived afterward. It is finally tested on a 1-kW prototype IPMSM and shows a good searching accuracy and dynamic performance while the system loss and torque ripple will not increase thanks to the virtualized signal injection.**

***Index Terms*—Interior permanent magnet synchronous machine (IPMSM), maximum efficiency per ampere (MEPA) control, optimal searching, virtual high-frequency signal injection (VHFSI).**

I. Introduction

INTERIOR permanent magnet synchronous machines (IPMSMs) are considered to be one of the most suitable drive machines for industry and home appliances due to its high efficiency, high torque density, and wide speed range performance [1]–[3]. It is noteworthy that the electric machine consumes 70% of global power energy. Even if the machine efficiency could be increased by 1%, it will save 26-TW·h electricity in China per annum. Consequently, the improvement of efficiency of IPMSM drive system has now become one of the most effective technologies for energy saving and cost-down of both industrial and civil consumptions [4]–[5]. Thus, researches on high-efficiency IPMSM control have been widely reported in recent articles [6]–[25].

Manuscript received March 5, 2019; revised June 14, 2019 and October 4, 2019; accepted October 31, 2019. Date of publication November 5, 2019; date of current version February 20, 2020. This work was supported in part by the Research Fund for the National Science Foundation of China under Grants 51707062, 51737004, 51575167 and 51877075 and in part by the National Key Research and Development Program of China under Grant 2018YFB0606000. Recommended for publication by Associate Editor J. Zhang. *(Corresponding author: Sheng Huang.)*

M. Li, X. Wu, and G. Liang are with the College of Electrical and Information Engineering, Hunan University, Changsha 410082, China (e-mail: hnuguangjing@163.com; wuxuan24@163.com; 809480380@qq.com).

S. Huang is with the Department of Electrical Engineering, Technical University of Denmark, 2800 Kgs. Lyngby, Denmark (e-mail: huang98123@163.com).

K. Liu and X. Peng are with the College of Mechanical and Vehicle Engineering, Hunan University, Changsha 410082, China (e-mail: lkan@hnu.edu.cn; xypeng@hnu.edu.cn).

Color versions of one or more of the figures in this article are available online at http://ieeexplore.ieee.org.

Digital Object Identifier 10.1109/TPEL.2019.2951754

As reported in the existing articles, the main-stream efficiency improvement technologies for IPMSM drive control are mainly divided into two categories [6]–[10]. The first one realizes the maximum output torque with the minimum current amplitude, also known as the maximum torque per ampere (MTPA) control [6]–[11]. The optimal current angle of MTPA can be obtained by using a pretested lookup table [7], [8] or online searching methods [9]–[11], being without requirements of prior knowledge of machine parameters. Although the MTPA method presents a better operation efficiency performance compared with $i_d = 0$ control. However, the MTPA method considers only minimum copper loss and, thus, makes it not applicable to maximum efficiency per ampere (MEPA) control. The MEPA method should consider all drive system losses [11], which is an alternative control algorithm for the IPMSM drive.

The other efficiency improvement method is based on the online tracking of MEPA point, which can be further classified as: loss model based method [12]–[15], hybrid optimal method [16]–[18], and online searching method [19]–[24]. The loss model based method retrieves the optimal combination of *dq*-axes reference currents from a pretested lookup table or a high-order polynomial approximation. For this kind of method, the accuracy of copper and iron loss mathematical models is the key factors. However, the loss model based method requires numerous repetitive experiments to form a lookup table including detailed machine loss information under all operation conditions, which suffers from disadvantages, such as time-consuming and huge computation burden [13]–[15]. Besides, the high-frequency machine loss and inverter loss are rarely considered in loss model based method, which results in an inevitable searching error. In order to solve the abovementioned issues, the online searching method has been proposed in recent articles, which could conduct an online searching of the minimum power loss of the IPMSM drive system. Compared with the loss model based method, it can effectively track the MEPA current angle, irrespective of the varying machine parameters. However, it should be noted that the online searching method has a relatively low convergence rate compared with the loss model based method and is easily affected by current or voltage harmonic. A comparative study of the aforementioned two methods has been discussed in [25].

Recently, the virtual signal injection (VSI) method has been reported in recent articles for MTPA control of IPMSMs, which can continuously derive the optimal current angle of MTPA

from a virtual machine torque model [26]–[29]. It only needs to inject high-frequency square or sine signals into the virtual machine model, and has no influence on the output torque and losses of the real electrical machine. Meanwhile, it has a quite low computation burden and is robust to parameter variations. Besides, owing to its simplicity in calculation, it could be used for online operation and also exhibits a good dynamic performance, especially when a virtual high-frequency square wave signal is employed [26]. Application of the VSI to the maximum efficiency control has been rarely reported so far. It is noticed that although the VSI method has been studied for MTPA tracking, but its maximum efficiency point tracking and robustness against inductance and flux linkage variations that can improve the IPMSM drive efficiency have not been properly studied and reported yet. Fast response and strong robustness against variations can ensure a fast current angle tracking with a good accuracy, which is important for the maximum efficiency operation of an IPMSM drive system. Introducing the virtual high-frequency signal injection (VHFSI) method to an IPMSM drive, explaining the implementation process and sufficient experimental verifications showing the accuracy of the MEPA point tracking are the new contributions of this article.

Therefore, aiming to solve the aforementioned issue, a VHFSI-based MEPA control method taking both loss models of IPMSM and inverter loss models into consideration is proposed in this article. It only needs to inject a virtual high-frequency signal into the loss models of the IPMSM and the inverter, and the optimal current angle could be online calculated. Since there is only one VSI to the loss model, it has no influence on the real losses and torque ripples of the IPMSM drive. Besides, extensive experimental investigations are conducted to validate the proposed MEPA tracking control scheme on a laboratory 1.0-kW IPMSM drive system, and it is found that the proposed method can achieve an accurate and fast MEPA control performance.

This article is organized as follows. Section II describes the IPMSM mathematical model and its loss model. The VHFSI algorithm based on the mathematical loss model of the IPMSM drive system is given in Section III. The experimental verification of the proposed scheme is introduced in Section IV. Finally, Section V concludes this article.

II. IPMSM Drive System Model Description

A. IPMSM Mathematical Model

The dynamic voltage equations of an IPMSM are represented in the *dq*-rotating reference frame [30], as

$$\begin{cases} u_{sd} = L_d \frac{di_d}{dt} + R_s i_d - w_e L_q i_q \\ u_{sq} = L_q \frac{di_q}{dt} + R_s i_q + w_e L_d i_d + w_e \lambda_m \end{cases} \tag{1}$$

where $u_{sd}$and u_{sq} are the stator voltages; $i_d$and i_q are the *dq*-axes currents; L_d and L_q are the *dq*-axes inductances; R_s is the stator winding resistance; λ_m is the rotor flux linkage; and w_e is the electric angular velocity.

The IPMSM electromagnetic torque and mechanical equations are expressed as

$$\begin{cases} T_e = \frac{3}{2} p(\lambda_m i_q + (L_d - L_q) i_d i_q) \\ J \frac{dw_m}{dt} = T_e - T_L - B w_m \end{cases} \tag{2}$$

where *p* is the number of pole pairs, w_m is the mechanical rotor speed and $w_e = p w_m$, T_L is the load torque, and *B* and *J* are the frictional coefficient and moment of inertia, respectively.

For the given reference current command I_s, the *dq*-axes currents $i_d$and i_q are presented as

$$\begin{cases} i_d = -I_s \sin(\gamma) \\ i_q = I_s \cos(\gamma) \end{cases} \tag{3}$$

where γ is the current angle between the stator current vector and the *q*-axis. The optimal current angle γ for the IPMSM drive has been studied in the literature [25]. If the machine parameters are known, the desired angle γ satisfies that $\partial T_e / \partial \gamma$ is equal to zero at constant current amplitude [26], which can be expressed as

$$\gamma = \sin^{-1} \frac{-\lambda_m + \sqrt{\lambda_m^2 + 8(L_q - L_d)^2 I_s^2}}{4(L_q - L_d) I_s}. \tag{4}$$

However, it is worth to point out that even though the precise machine parameters are used in (4), accurate MEPA control still cannot be achieved. This is due to the neglecting of the iron loss, high-frequency loss and inverter loss in the IPMSM drive system. The MTPA method considers only the copper loss while minimizing the current amplitude for the same torque.

B. Loss Model and System Efficiency

An accurate and fast total losses calculation method is crucial for MEPA operation. Therefore, the loss model characteristics of the IPMSM drive system considering the fundamental frequency loss, high-frequency loss and inverter loss are presented in this section. An efficiency calculation method is developed with parameter independence to the machine inductance and flux linkage.

The fundamental frequency loss of IPMSM includes the copper loss $P_{\mathrm{cu},f}$ and the iron loss $P_{\mathrm{ir},f}$ [13], in which $P_{\mathrm{cu},f}$ can be represented as

$$P_{\mathrm{cu},f} = \frac{3}{2} R_s I_s^2 = \frac{3}{2} R_s (i_d^2 + i_q^2). \tag{5}$$

From (5), $P_{\mathrm{cu},f}$ is related to the phase current amplitude, whereas the resistance R_s is affected by the operation temperature.

The iron loss can be classified as teeth iron loss and yoke iron loss. The stator teeth, yoke flux density, and operation frequency decide the iron loss $P_{\mathrm{ir},f}$ together. The iron loss per volume can be written as follows

$$dP_{\mathrm{ir},f} = \sigma_h B_m^2 f + \sigma_e B_m^2 f^2 \tag{6}$$

$$\sigma_e = \frac{\pi^2 \sigma k_d^2}{6} \tag{7}$$

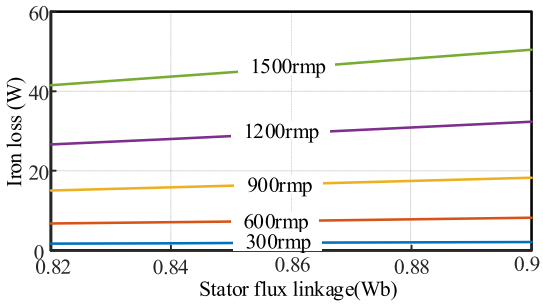

Fig. 1. Iron loss under different stator flux linkage and speed.

TABLE II
IPMSM SPECIFICATIONS

Parameters of IPMSM			
Rated power(w)	1000	Stator resistance (Ω)	3.98
Phase voltage (V)	253	*d*-axis inductance (mH)	33.08
Rated current (A)	2.7	*q*-axis inductance (mH)	111.93
Rated speed (r/min)	1000	PM flux linkage (Wb)	0.824
Rated frequency (Hz)	33.3	Pole pairs	2

where B_m is the flux density and f is the machine operation frequency. σ_h and σ_e are the hysteresis and eddy loss coefficient, respectively. σ_h depends on the material property. K_d is the thickness of laminated steel. σ is the electrical conductivity of laminated steel.

The total iron loss including the teeth and yoke losses can be defined in the *dq*-frame as

$$P_{\mathrm{ir},f} = dP^{f}_{\mathrm{irt},dq}V_t + dP^{f}_{\mathrm{iry},dq}V_y \tag{8}$$

where V_t and V_y are the volume of machine teeth and yoke, respectively. A_t and A_y are the areas of machine teeth and yoke, respectively. The flux density on the teeth $B_{t,dq}$ and yoke $B_{y,dq}$ can be expressed with the stator flux linkage as

$$B_{t,dq} = \sqrt{\lambda^2_{md} + \lambda^2_{mq}}/A_t, B_{y,dq} = \sqrt{\lambda^2_{md} + \lambda^2_{mq}}/A_y. \tag{9}$$

The total fundamental frequency iron loss (8) can be expressed by using (6) and (9) as

$$P_{\mathrm{ir},f} = \sigma_{Hc} f\left(\lambda^2_{md} + \lambda^2_{mq}\right) + \sigma_{Ec} f^2\left(\lambda^2_{md} + \lambda^2_{mq}\right) \tag{10}$$

$$\sigma_{Hc} = \sigma_h\left(\frac{V_t}{A_t^2} + \frac{V_y}{A_y^2}\right), \sigma_{Ec} = \frac{\pi^2\sigma k_d^2}{6}\left(\frac{V_t}{A_t^2} + \frac{V_y}{A_y^2}\right). \tag{11}$$

The iron loss coefficients are required to calculate the iron loss using experiment method. First, small i_q current is used to compensate the mechanical losses under $i_d = 0$ at various speeds. The machine operates at different speeds from no-load to full-load. The measured iron loss of the electrical machine can be obtained by subtracting the copper loss, high frequency loss, and inverter loss from the total losses. The iron loss coefficients can be obtained by using curve fitting method. The constants σ_{Hc} and σ_{Ec} are the measured average values under five different speeds and flux linkage values. The measured iron loss is shown in Fig. 1. The tested IPMSM parameters are given in Table II. It can be derived from the obtained results that the average value of σ_{Hc} and σ_{Ec} are 0.027 and 0.014, respectively, and they will be used in this article.

TABLE I
TECHNICAL DATA FOR IGBT MODULE AT TEMPERATURE 25°C

Variable	Typical value	Unit
E_{on} (I_c=25A, V_{cc}=600V)	33	mJ
E_{off} (I_c=25A, V_{cc}=600V)	56	mJ
E_{err} (I_f=25A, $-\mathrm{d}I_f/dt$= 1100A/us)	30.5	mJ
R_{on}	0.5	mΩ
V_{on}	1.5	V

The high-frequency loss of the IPMSM system produced by nonsinusoidal power supply is inevitable, which makes the loss increase, especially due to the switching frequency harmonic. The harmonic eddy loss $P_{\mathrm{el,h}}$ is one of the main components, whereas the harmonic copper loss can be neglected [31]. It can be expressed as

$$P_{\mathrm{el,h}} = k_{\mathrm{el,h}}\Delta V^2_{\mathrm{rms}} \tag{12}$$

$$\Delta V^2_{\mathrm{rms}} = \frac{V^2_{\mathrm{dc}}}{3}\left(\frac{2}{\pi}M_a - \frac{1}{2}M_a^2\right) \tag{13}$$

where V_{dc} is the dc-link voltage, and M_a is the voltage modulation coefficient. In this article, the loss coefficient $k_{\mathrm{el,h}}$ is selected to be 0.001 and it can be obtained by using finite element analysis (software Maxwell) under voltage source supply [32].

The main losses on the inverter are the conduction loss $P_{\mathrm{inv,con}}$ and switching loss $P_{\mathrm{inv,sw}}$ [32], which are expressed as

$$P_{\mathrm{inv,sw}} = \frac{6}{\pi}(E_{\mathrm{on}} + E_{\mathrm{off}} + E_{\mathrm{err}})f_{\mathrm{sw}}V_{\mathrm{dc}}I_s \tag{14}$$

$$P_{\mathrm{inv,con}} = 6\left(\frac{1}{\pi}V_{\mathrm{on}}I_s + \frac{1}{4}R_{\mathrm{on}}I_s^2\right) \tag{15}$$

where f_{sw} is the switching frequency. E_{on} and E_{off} are the energy required to turn ON and turn OFF an insulated gate bipolar transistor (IGBT), respectively. E_{err} is the power consumed during the diode turning-OFF period. R_{on} and V_{on} are the resistance and forward threshold voltage, respectively. For the power module, the Infineon IGBT module FS25R12KE3 is used on the tested drive and the datasheet is given in Table I.

Hence, the total losses can be expressed as

$$P_{\mathrm{loss,total}} = P_{\mathrm{cu},f} + P_{\mathrm{ir},f} + P_{\mathrm{el},h} + P_{\mathrm{inv,sw}} + P_{\mathrm{inv,con}}. \tag{16}$$

The inverter input power can be calculated by

$$P_{\mathrm{in}} = 1.5 \times (u_{sd}i_d + u_{sq}i_q) \tag{17}$$

where u_{sd} and u_{sq} are the reference voltages of the current loop outputs. Hence, the efficiency of the IPMSM drive system can be derived as

$$\eta = \frac{P_{\mathrm{in}} - P_{\mathrm{loss,total}}}{P_{\mathrm{in}}}. \tag{18}$$

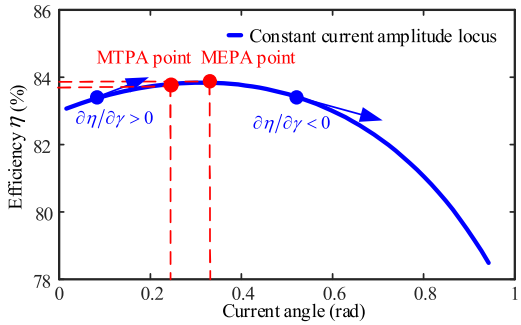

Fig. 2. Relationship between the current angle and the efficiency under fixed current amplitude.

III. Proposed Virtual HF Signal Injection Method for Maximum Efficiency Tracking

This section proposes a novel MEPA point tracking method for the IPMSM drive system, in which the virtual HF square wave signal is injected to the mathematical model to obtain the optimal current angle. In this way, the MEPA angle can be extracted from the derived MEPA equation. The proposed scheme is robust to inductance and flux linkage parameter variations and the dynamic response is not sacrificed. The implementation procedure of the proposed method is introduced in this section.

A. Searching for the MEPA Point Using Virtual HF Signal Injection

The theoretical efficiency curve of the tested IPMSM is shown in Fig. 2. The nameplate data of this machine are given in Table II. The curve is obtained with a fixed current amplitude 2.7 A using a sweeping current angle method. With the current angle changing from 0 to 1 rad, the efficiency initially increases to the maximum value and then decreases. The maximum value is called the MEPA point and it satisfies condition $\partial\eta/\partial\gamma = 0$. There is a difference between MEPA point and MTPA point. Besides, the machine parameters, such as inductance and magnet flux linkage, are easily affected due to magnetic saturation and temperature rise. Thus, the MEPA point calculated by using machine datasheet parameters is inaccurate. Therefore, a VHFSI method is proposed for online tracking the MEPA angle in this article.

First, a square waveform signal is injected to the current angle with 50% duty cycle, which is expressed as

$$\beta(t) = \begin{cases} A, & kT_s \le t < (k+1/2)T_s \\ 0, & (k+1/2)T_s \le t < (k+1)T_s \end{cases} \tag{19}$$

where A is the amplitude of the injected square waveform and T_s is the period of the injection signal. k represents the nature sequence.

Taylor's series expansion of the efficiency after the VSI can be derived as

$$\begin{aligned} \eta^h(\beta) &= \eta^h(0) + \frac{\partial\eta^h}{\partial\beta}|_{\beta=0}\beta + \frac{1}{2}\frac{\partial^2\eta^h}{\partial^2\beta}|_{\beta=0}\beta^2 + \cdots \\ &= \eta(\gamma) + \frac{\partial\eta}{\partial\gamma}\beta + \frac{1}{2}\frac{\partial^2\eta}{\partial^2\gamma}\beta^2 + \cdots \end{aligned} \tag{20}$$

where the superscript h represents the symbol of the injected signal. To simplify the analysis, the fundamental component of (20) is the major variation of the efficiency. Therefore, the high-order components could be ignored. In this case, (20) can be rewritten as

$$\eta^h(\beta) = \eta(\gamma) + \frac{\partial\eta}{\partial\gamma}\beta. \tag{21}$$

In (21), $\eta(\gamma)$ represents the drive system efficiency without the injection signal, which can be calculated by using (18). Thus, the searching objective is transferred from the MEPA point to the point at $\partial\eta/\partial\gamma = 0$.

Since the injected signal β is a quite small value, thus, it satisfies $\cos\beta \approx 1$ and $\sin\beta \approx \beta$. The current i_d^h and i_q^h after signal injection can be expressed as

$$i_d^h = -I_s\sin(\gamma+\beta) = i_d\cos\beta - i_q\sin\beta \approx i_d - i_q\beta \tag{22}$$

$$i_q^h = I_s\cos(\gamma+\beta) = i_q\cos(\beta) + i_d\sin(\beta) \approx i_q + i_d\beta. \tag{23}$$

After injecting the signal, the current will induce input power change, which is (24) according to the model (17)

$$P_{\text{in}}^h = \frac{3}{2}(u_{sd}i_d^h + u_{sq}i_q^h). \tag{24}$$

Substituting (22) and (23) into (24) and, thus, (24) can be simplified to

$$P_{\text{in}}^h = \frac{3}{2}\left[u_{sd}i_d + u_{sq}i_q + (u_{sq}i_d - u_{sd}i_q)\beta\right]. \tag{25}$$

In order to calculate accurately the IPMSM system efficiency, the loss model after signal injection should be considered. The fundamental frequency copper loss with the injected signal can be written as

$$P_{cl}^h = R_s((i_d^h)^2 + (i_q^h)^2) = R_s(1+\beta^2)(i_d^2 + i_q^2). \tag{26}$$

The accuracy of iron loss depends on the accurate stator flux linkage value. However, the machine parameters can change due to magnetic saturation and temperature rise. Thus, the stator flux linkage may not be accurately calculated by using the nominal inductance and flux linkage values. Hence, the stator flux linkage could be estimated from the voltage and current. By neglecting the current differential terms associated with the inductance, the stator flux linkage can be obtained from the voltage as

$$\begin{cases} \lambda_{md} = \frac{u_{sq} - R_s i_q}{w_e} \\ \lambda_{mq} = \frac{-u_{sd} + R_s i_d}{w_e}. \end{cases} \tag{27}$$

Because R_s can be updated online as discussed in Section III-B, the iron loss model is robust against inductance and flux linkage parameters variations. The stator flux linkage after signal injection can be expressed as

$$\begin{cases} \lambda_{md}^h = \frac{u_{sq} - R_s i_q^h}{w_e} = \frac{u_{sq} - R_s(i_q + i_d\beta)}{w_e} \\ \lambda_{mq}^h = \frac{-u_{sd} + R_s i_d^h}{w_e} = \frac{-u_{sd} + R_s(i_d - i_q\beta)}{w_e}. \end{cases} \tag{28}$$

Hence, the fundamental iron loss can be derived as

$$P_{\text{ir}}^{f,h} = \sigma_{Hc}f((\lambda_{md}^h)^2 + (\lambda_{mq}^h)^2) + \sigma_{Ec}f^2((\lambda_{md}^h)^2 + (\lambda_{mq}^h)^2). \tag{29}$$

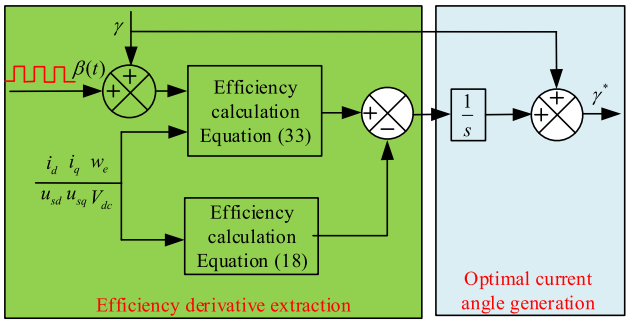

Fig. 3. Schematic of the optimal current angle generation technique.

The constant σ_{Hc} and σ_{Ec} can still use the values obtained from the measured results as discussed previously. The high-frequency eddy iron loss depends on the voltage, which is kept unchanged. The inverter loss after signal injection can be expressed as

$$P^h_{\text{inv,sw}} = \frac{6}{\pi}(E_{\text{on}} + E_{\text{off}} + E_{\text{err}}) f_s V_{\text{dc}} \sqrt{(i^h_d)^2 + (i^h_q)^2} = \frac{6}{\pi}(E_{\text{on}} + E_{\text{off}} + E_{\text{err}}) \sqrt{1+\beta^2} f_s V_{\text{dc}} I_s \quad (30)$$

$$P^h_{\text{inv,con}} = 6\left(\frac{1}{\pi} V_{\text{on}} \sqrt{1+\beta^2} I_s + \frac{1}{4} R_{\text{on}} (1+\beta^2) I_s^2\right). \quad (31)$$

The total loss of the drive system after signal injection can be derived as

$$P^h_{\text{loss,total}} = P^h_{\text{cu},f} + P^h_{\text{ir},f} + P_{\text{el,h}} + P^h_{\text{inv,sw}} + P^h_{\text{inv,con}}. \quad (32)$$

Hence, the efficiency η^h can be expressed as

$$\eta^h = \frac{P^h_{\text{in}} - P^h_{\text{loss,total}}}{P^h_{\text{in}}}. \quad (33)$$

The searching objective value $\beta \partial \eta / \partial \gamma$ can be obtained by combining (17), (18), (21), and (33) as

$$\frac{\partial \eta}{\partial \gamma} \beta(t) = \begin{cases} \frac{\partial \eta}{\partial \gamma} A, kT_s \le t < (k+1/2)T_s \\ 0, (k+1/2)T_s \le t < (k+1)T_s. \end{cases} \quad (34)$$

The maximum value of $\frac{\partial \eta}{\partial \gamma}\beta(t)$ is updated online on each pulsewidth modulation (PWM) period. A pure integral is used to track the MEPA optimal current angle with an initial value. The initial angle is chosen to be the MTPA angle because MTPA angle is very close to the MEPA angle and this will reduce the convergence time. The detailed implementation scheme of the VSI method is illustrated in Fig. 3.

The optimal current angle can be obtained from the aforementioned method. The d-axis and q-axis current references could be expressed as

$$\begin{cases} i^*_d = -I_s \sin(\gamma *) \\ i^*_q = I_s \cos(\gamma *). \end{cases} \quad (35)$$

Thus, the proposed MEPA method can realize an accurate current control for the IPMSM drive system with a simple implementation and fast response. The d-axis and q-axis feedback currents are used to track the reference values accurately.

B. Implementation Procedure

The proposed VSI scheme for searching the MEPA point of the IPMSM drive system is implemented. The specifications of the experimental IPMSM are listed in Table II. From (18), the dq-axes currents, dq-axes reference voltages, machine rotational speed, and the optimal current angle need to be measured in each PWM period for calculating the maximum efficiency point.

The copper loss is directly calculated according to the feedback dq-axes currents. The stator resistance R^T_s may change with the operation temperature, which can be expressed as

$$R^T_s = R_s(1 + \alpha(T - T_0)) \quad (36)$$

where R_s is the initial resistance at room temperature T_0. The actual temperature T can be detected by the thermal resistor placed in the windings. α is the thermal coefficient of the copper. The iron loss for the fundamental frequency is calculated by (10), so it has to ensure that the correct flux density value is used. The reference voltage u_{sd} and u_{sq} are the current loop control outputs and are taken as the measured voltage. However, the inverter terminal voltage may be different from the reference voltage due to the inverter nonlinear effects, such as dead time and diode voltage drop. Therefore, the reference voltage has to be compensated for reducing the input power error. The revised reference voltage can be expressed as

$$\begin{bmatrix} u^*_d \\ u^*_q \end{bmatrix} = \begin{bmatrix} u_{sd} \\ u_{sq} \end{bmatrix} + V_{\text{dead}} \begin{bmatrix} D_d \\ D_q \end{bmatrix} \quad (37)$$

where D_d and D_q can be expressed as

$$\begin{bmatrix} D_d \\ D_q \end{bmatrix} = 2 \begin{bmatrix} \cos(\theta) & \cos(\theta - 2/3\pi) & \cos(\theta + 2/3\pi) \\ -\sin(\theta) & -\sin(\theta - 2/3\pi) & \sin(\theta - 1/3\pi) \end{bmatrix} \times \begin{bmatrix} \text{sign}(i_a) \\ \text{sign}(i_b) \\ \text{sign}(i_c) \end{bmatrix}. \quad (38)$$

In (38), D_d and D_q present periodic variation with the rotor position θ. Therefore, the average value u^*_d and u^*_q should be used for power calculation. The distorted voltage V_{dead} is a constant of 0.5 V for the tested system. The modulation index M_a is used to calculate the high-frequency eddy current loss. M_a is calculated using (39). The measured dc-link voltage and current are used to calculate the inverter loss according to the inverter loss model (14) and (15)

$$M_a = \frac{2V_{\text{line}}}{V_{\text{dc}}} = \frac{2\sqrt{u^{*2}_d + u^{*2}_q}}{V_{\text{dc}}}. \quad (39)$$

The VSI method for searching the optimal current angle is summarized as follows. The flowchart of the implementation procedure is given in Fig. 4 and the drive system control flowchart is given in Fig. 5.

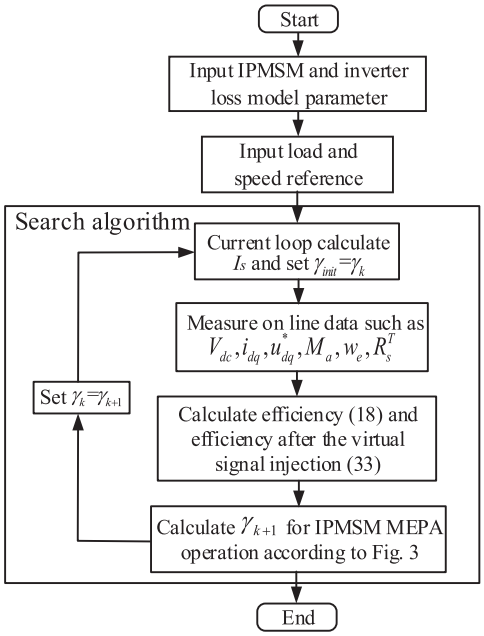

Fig. 4. Flowchart of the implementation procedure of MEPA operation for an IPMSM drive system based on the VSI method.

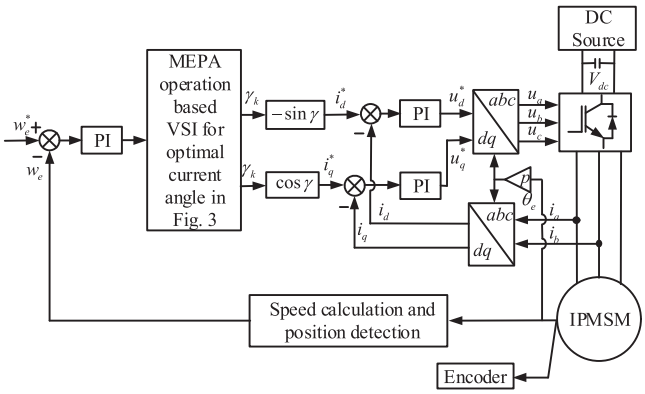

Fig. 5. System control block diagram of IPMSM MEPA operation with the VSI method.

VSI method based MEPA operation of IPMSM using optimal current angle γ.

1. Set initiate parameters, such as the current angle γ_{init}, R_s, loss model constant, and set $k = 1$.
2. Measure V_{dc}, i_{dq}, u^*_{dq}, M_a, w_e, and R^T_s with the temperature T.
3. Calculate the efficiency using (18), the VSI efficiency using (33), and the optimal angle $\gamma_{\text{opt}}(k+1)$.
4. Obtain new reference current command i^*_{dq}, set $k = k+1$ and go back to 2.

The needed data for online losses calculation during the PWM period could be directly obtained, which are simple and effective. Besides, this calculation method is very robust to current/voltage harmonics and machine parameter (inductance and flux linkage) variations. The efficiency calculation is reliable since the loss model considers all loss components including both the machine and the inverter. Moreover, the injection signal is not real, thus, it will not result in any negative effect, such as increased loss and torque ripple. Furthermore, the square signal injection method does not require any filters. Therefore, the system exhibits fast dynamic response and good stability. The updated γ_{opt} could be used to realize the maximum efficiency operation for IPMSM drive system with the minimum energy consumption.

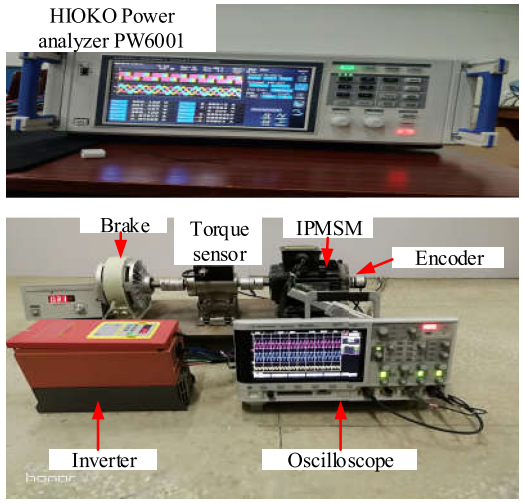

Fig. 6. Experimental platform for verifying the proposed MEPA operation method.

IV. Experimental Verifications

The proposed algorithm is validated on a 1.0-kW IPMSM drive system. The IPMSM parameters are given in Table II. A mechanically coupled magnetic powder brake (see Fig. 6) is employed as the external load in the test bench. The algorithm is implemented on a DEMA D6L inverter, which includes a fixed point Texas Instrument (Dallas, TX, USA) processor (DSP-F2808) controller. An incremental encoder PEN K3808G-2000BM-K830 with 2000 P/R resolution is used for measuring the rotor position and speed. In the experiment, the sampling and switching frequency of the SVPWM is set to 10 kHz. In order to minimize the effect between fundamental frequency and injected virtual signal current angle, the frequency of virtual injected signal should be selected as high as possible. However, it could not exceed the switching frequency. Therefore, the virtual injected signal amplitude is selected 0.002 rad with 50% duty cycle and the injected frequency is set to 1 kHz in this article. The dc-link voltage through a three-phase uncontrollable rectifier is 580 V. The initial resistance is tested before starting the experiment. Then, the stator resistance is updated online in the program according to the detected temperature by using (36). The speed loop PI regulator (with $k_p = 50$ and $k_i = 200$) and the current loop PI regulator (with $k_p = 30$ and $k_i = 30$) are used in the controller.

The first set experiment is conducted to find the actual MEPA angle using the sweeping method at the rated current. A torque sensor (JN338-50) with a resolution of 0.1% between the IPMSM and the brake is installed to measure the output

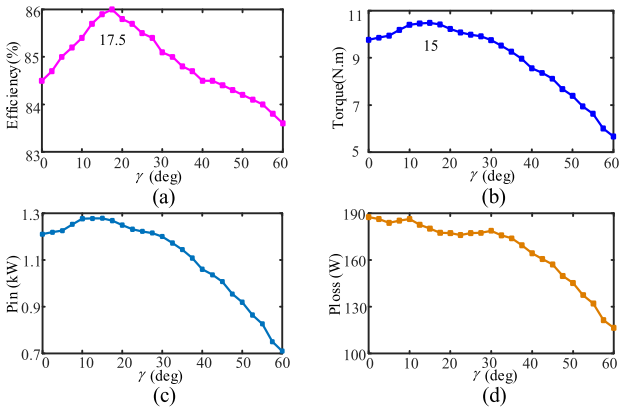

Fig. 7. Current angle sweep result at 1000 r/min and $I_s = 2.7$A. (a) Efficiency versus current angle. (b) Torque versus current angle. (c) Input power versus current angle. (d) Total loss power versus current angle.

mechanical torque and calculate the output power. The power analyzer HIOKI PW6001 with an accuracy of $\pm 0.02\%$ is used for the input power measurement. This actual current angle can be used to compare and evaluate the accuracy of the proposed algorithm with the tracking results in the later section. The detailed test process for obtaining the actual MEPA angle is divided into the following steps.

Test process for actual MEPA current angle Υ.
Step.1: Initial operation condition, speed $w_r = 1000$r/min, $\Upsilon_0 = 0$, increase the load until the current reach $I_s = 2.7$A.
Step.2: Measure the mechanic power P_{out} and the input power P_{in}. Calculate the efficiency $\eta = P_{\text{out}}/P_{\text{in}}$.
Step.3: $\gamma_{k+1} = \Upsilon_k + 0.25$deg, adjust the load and keep the current $I_s = 2.7$A.
Step.4: Repeat Step 2 and Step 3 till $\Upsilon = 60$deg. Find the actually optimal MEPA current angle Υ. End

Fig. 7 presents the sweeping current angle results of efficiency, torque, input power, and total power loss at rated current of 2.7 A and the rated speed of 1000 r/min. It can be seen that the current angle for the maximum efficiency point is 17.5°, whereas for the MTPA operation, the current angle is 15°. The difference between the MEPA angle and the MTPA angle is due to the neglecting of the iron loss, eddy loss, and inverter loss in MTPA. Therefore, the accurate MEPA tracking method is required to obtain maximum efficiency operation point.

In order to verify the accuracy of loss model, the measured and analytically calculated efficiency values with the MEPA control on the tested IPMSM drive system at 1000 r/min are compared in Fig. 8. The current angle of the measured efficiency is the same as the calculated efficiency. The test time is short enough to keep the operation temperature and the resistance similar between the comparison experiments. It can been seen that the maximum efficiency error between the measured and calculated efficiency is less than 0.5%. Therefore, the proposed method is precise enough for loss model.

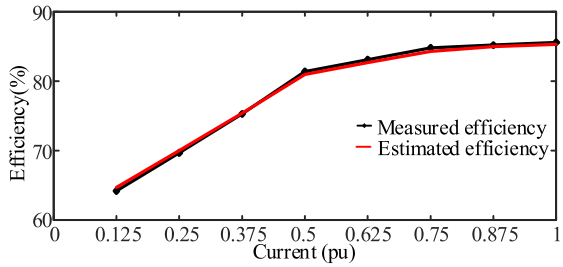

Fig. 8. Comparison of the MEPA efficiency obtained from the measured results and analytical calculation.

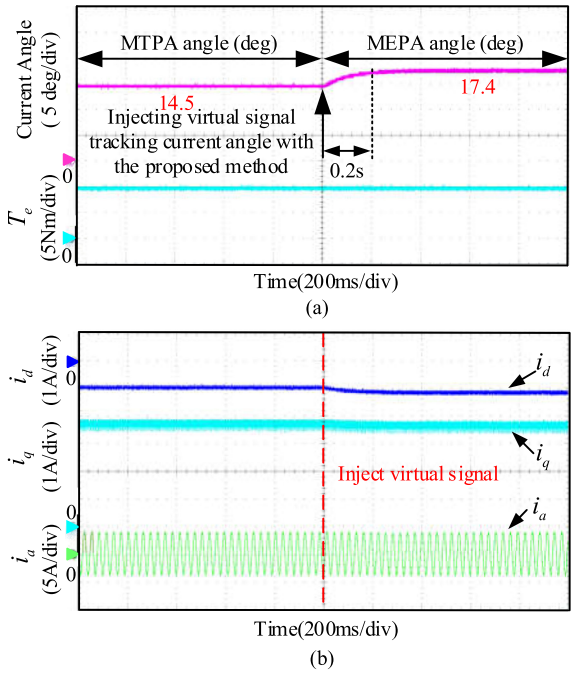

Fig. 9. Current angle tracking to search the MEPA angle at 1000 r/min and rated load; initial current angle of 14.5°. (a) Current angle. (b) *dq*-axes current.

A. *MEPA Tracking With the Proposed Approach*

In this experiment, the performance of tracking the MEPA angle is validated with the proposed VSI method. When the IPMSM enters a steady state, the virtual signal angle $\beta(t)$ is injected into the initial angle to obtain the virtual efficiency, and the MEPA angle is then exacted by using the proposed algorithm in Fig. 3. In this test, the stator current is at its rated value of 2.7 A.

Fig. 9(a) shows the current angle, torque waveform and Fig. 9(b) shows the measured *dq*-axes current responses with the proposed method to track the MEPA point. After the square waveform signal is injected, the proposed algorithm is enabled at 1 s under the steady state. The initial current angle γ_{init} is set to 14.5° according to the MTPA (4) and machine parameters given in Table II. It can be seen that it takes 0.2 s to converge to the finial MEPA angle 17.4°. The MEPA angle of 17.4° is very close to the results obtained from the angle sweeping 17.5° at the speed of 1000 r/min and rated load. Therefore, the error between the real MEPA angle and the calculated MEPA angle is

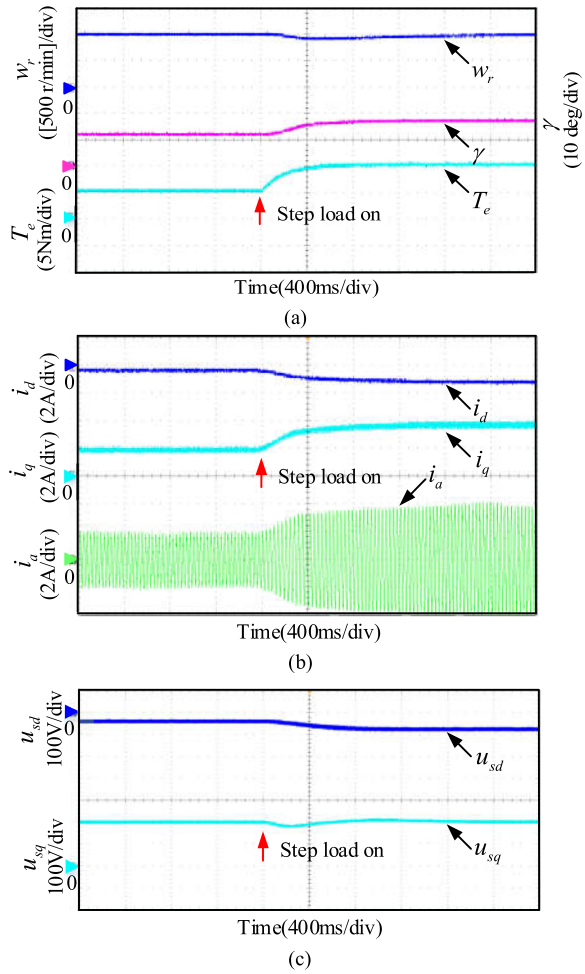

Fig. 10. Response of the proposed method to search MEPA point during the load change from 50% to 100% load at 1000 r/min. (a) Current angle and speed. (b) *dq*-axes current and phase A current. (c) *dq*-axes voltage.

0.1°, which is negligible. Besides, it can be seen that the VSI will not cause additional torque ripple. Hence, the proposed method is verified to be feasible for tracking the MEPA angle of the IPMSM drive system.

B. MEPA Tracking Load Change Experiment

In this experiment, the proposed method is investigated for the performance under different load conditions. Fig. 10(a) shows the calculated current angle, speed, and torque when the load step increases from 50% to 100% and the speed is maintained at 1000 r/min. Fig. 10(b) and (c) shows the *dq*-axes currents and voltage during the step load change. The initial calculated current angle is 12° with the MEPA method at 50% load. Then, when the load increases at 1.6 s, the current angle changes from 12° to 17.5° at 2.0 s. The current angle finally converges to the sweeping results. Besides, the quantitative comparison of the proposed MEPA angle $\gamma_{\rm calc}$ and the optimal sweeping current angle $\gamma_{\rm actual}$ under different currents are presented in Table III. From these results, the error between the calculation result and sweeping result is less than 1°. It can be seen that the proposed method could search for the MEPA point accurately with different load.

TABLE III
ACTUAL AND CALCULATED MEPA ANGLE AT 1000 r/min, VARYING I_s

I_s	0.25p.u.	0.5p.u.	0.75p.u.	1p.u.
γ_{calc}	8.4	11.7	14.8	17.2
γ_{actual}	8.9	12.4	15.3	17.5

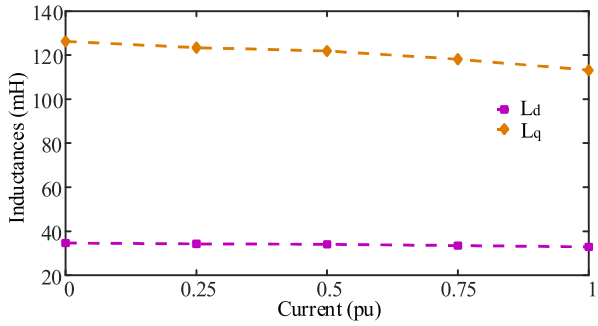

Fig. 11. Variation of *dq*-axes inductances of test machine under MEPA control.

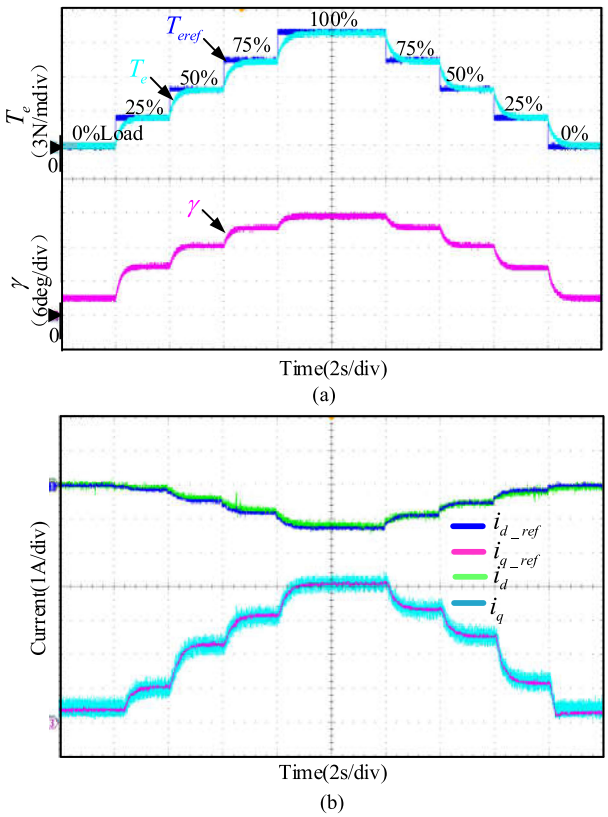

Fig. 12. Measured results of the proposed method at 1000 r/min. (a) Torque and current angle at 1000 r/min. (b) *dq*-axes current at 1000 r/min.

The variation of *dq*-axes inductances of the test machine under MEPA control is shown in Fig. 11. The machine inductance would change significantly from no-load to full-load. The rare earth permanent magnet (PM) XG196/96 with maximum working temperature of 120 °C is used for permanent magnets. Fig. 12 shows the experimental results of the proposed method

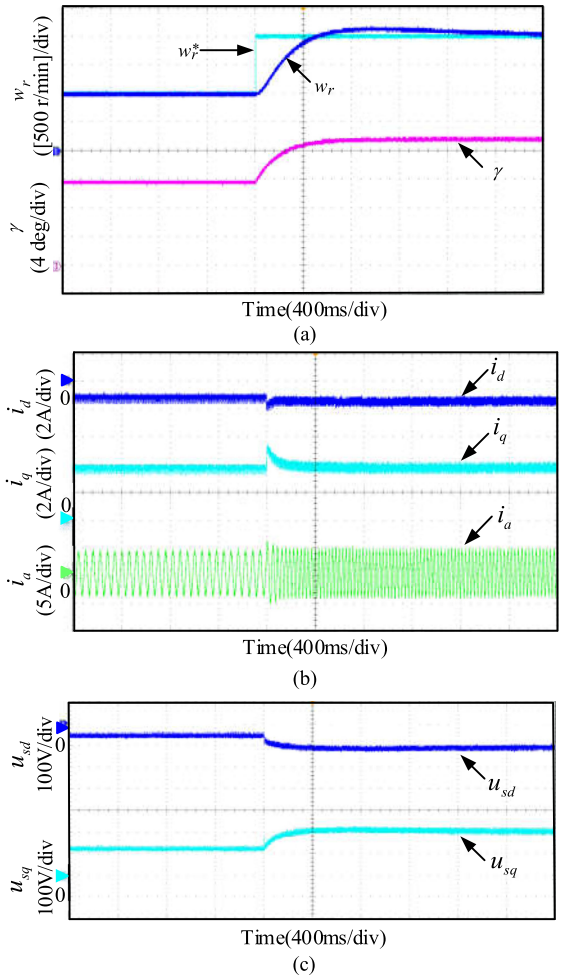

Fig. 13. Response of the proposed method to search MEPA point during the speed change from 500 to 1000 r/min at rated load. (a) Current angle and speed. (b) *dq*-axes current and phase A current. (c) *dq*-axes voltage.

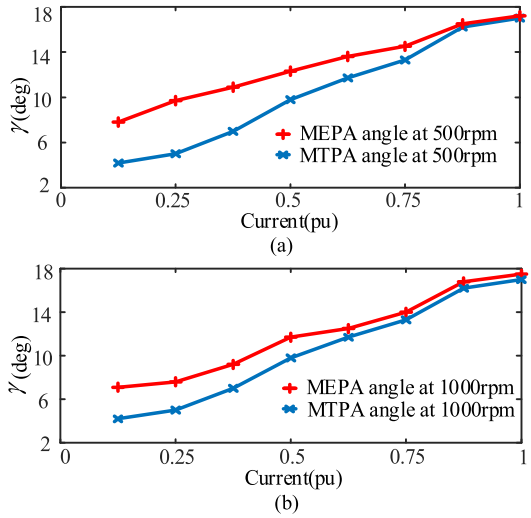

Fig. 14. Comparison of current angle under MTPA and proposed MEPA control method for varying current amplitude at two typical speeds and 25 °C operation temperature. (a) Current angle at 500 r/min with varying I_s. (b) Current angle at 1000 r/min with varying I_s.

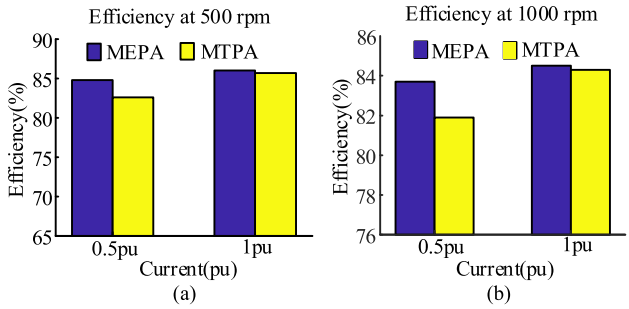

Fig. 15. Comparison of efficiency under MTPA and proposed MEPA control method at 0.5 and 1 p.u. current amplitude. (a) Efficiency at 500 r/min. (b) Efficiency at 1000 r/min.

at 1000 r/min with different step load changes. With introducing VSI, it can be observed that the current angle can track the MEPA point accurately and fast. The *dq*-axes current feedbacks can track the reference signals with fast responses. The proposed control scheme has good robustness against machine inductance and flux linkage variations.

C. MEPA Tracking Acceleration Experiment

In this experiment, the proposed method is investigated for the performance under different speeds. Fig. 13 shows the results of the proposed method when the speed step increases from 500 to 1000 r/min and the load is maintained at full load. Fig. 13(a) shows the results of the speed and current angle. Fig. 13(b) and (c) shows the *dq*-axes currents and voltages during the speed change. By varying the speed, the MEPA angle changes from 11° to 17.5° due to the increase of the iron loss and high-frequency eddy current loss. The calculated MEPA angle at 500 r/min is 11° and the real one is 12°. This indicates that the proposed VSI algorithm is feasible and can perform as expected under range speed condition.

D. MEPA Tracking Comparative Experiment With MTPA

Fig. 14 shows the comparison results of current angle with the MTPA method and the proposed MEPA method under different current amplitude at speeds of 500 and 1000 r/min. To make it a fair comparison between the MTPA result and the MEPA result, the operation temperature is selected at 25 °C and the current amplitude is strictly the same. It can be seen from Fig. 14 that the MEPA angle and MTPA angle increase with the load current amplitude until its rated value. Besides, the angle error is relatively large when the current amplitude is small.

Fig. 15 shows the measured efficiency comparison at 500 and 1000 r/min and 0.5 and 1 p.u. current, respectively. It can be seen from Fig. 15 that the proposed MEPA algorithm improves the system efficiency to a certain extent, especially in the low current load region.

Fig. 16(a) shows the system efficiency comparison under MEPA angle and MPTA angle with varying current and speed. Fig. 16(b) shows the efficiency improvement when using the MEPA angle to replace the MTPA angle. It can be seen that the efficiency in the high-speed range is improved more significantly

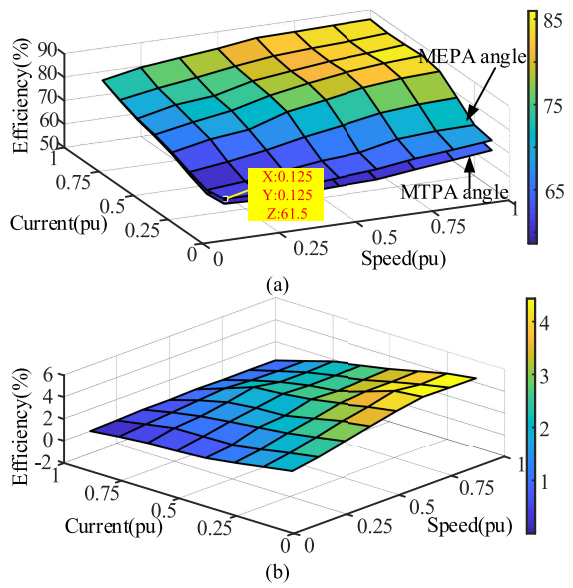

Fig. 16. Measured system efficiency at MEPA and MTPA current angle for various speed and current amplitudes. (a) Efficiency map of MEPA and MTPA. (b) Efficiency improvement of MEPA compared with MTPA.

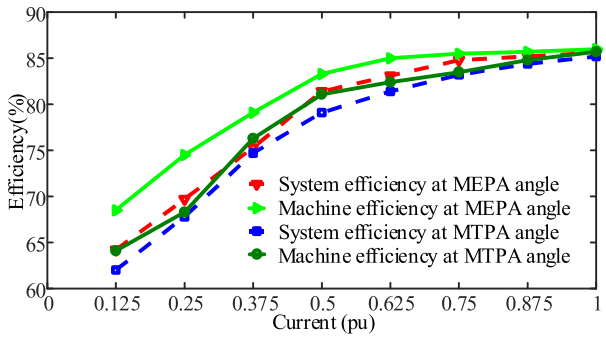

Fig. 17. System efficiency and machine efficiency under MEPA angle and MTPA angle at speed of 1000 r/min and varying I_s.

with the proposed method. For the low speed and high load condition, there has not much difference on the efficiency whatever current angle is used. When the proposed method is used, the efficiency could be improved in the whole operation range with different currents and speeds. It can be inferred that the energy saving benefit could be further clear for the high power machine and inverter with the proposed method.

Fig. 17 shows the measured efficiency of the system and machine at 1000 r/min with different load using the MEPA angle or the MTPA angle. It can be seen that the efficiency for both system and machine with the MTPA angle is a bit lower than that with MEPA angle at the same load condition. Table IV lists the loss comparison of MEPA and MTPA angles at the current of 0.25, 0.5, and 1 p.u., respectively, and the speed is kept at 1000 r/min. The copper loss is kept the same for both methods since the current amplitude does not change. It can be seen that the core loss increase with load current and the proposed MEPA method has a lower core loss. There is a slight increase in harmonic loss due to the increase of M_a. As the current increases from 0.25 to 1 p.u., the inverter loss with MEPA is slightly more

TABLE IV
LOSS COMPARISON AT 0.25, 0.5, AND 1 p.u. CURRENT AND 1000 r/min

I_s		0.25p.u.		0.5p.u.		1p.u.	
Method		MTPA	MEPA	MTPA	MEPA	MTPA	MEPA
Loss (W)	Copper	5.5	5.5	21.9	21.9	87.5	87.5
	Core	32.4	28.5	32.9	28.7	35.7	30.8
	Eddy	22.7	22.9	25.7	25.5	31.7	31.8
	Inverter	48.3	42.7	70.4	74.6	108	112
Efficiency improvement with the proposed method (%)		4.4		3.2		0.3	

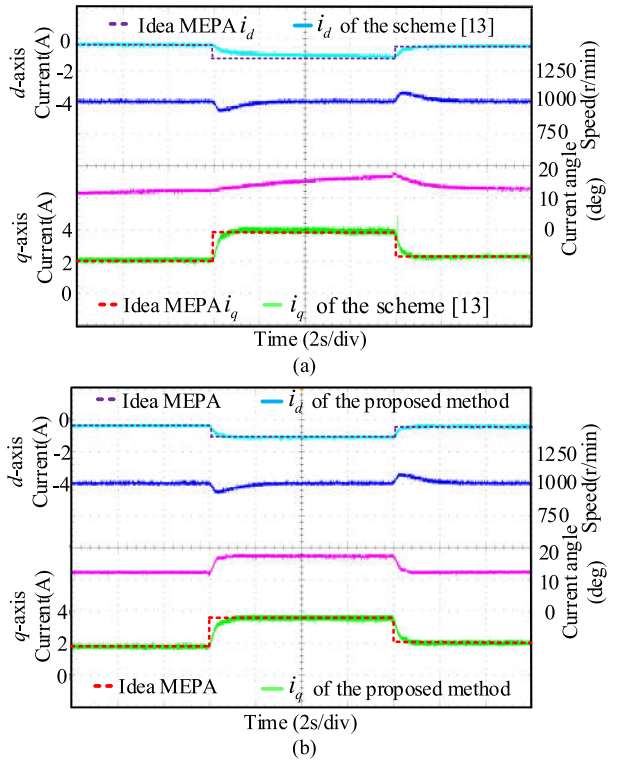

Fig. 18. Experimental results at 1000 r/min with step load change from 5 to 10 N·m and then to 5 N·m. (a) Method reported in [13]. (b) Proposed method.

than that of MTPA method at 0.25 p.u. and then less than it at 0.5 and 1 p.u. Besides, it can be seen that the total efficiency improvement is more significant in the low current region.

E. MEPA Tracking Comparative Experiment With Method Reported in [13]

To prove the dynamic performance of the proposed method, the experimental results of *dq*-axes currents and the speed response at the speed of 1000 r/min with step load changes of 5–10–5 N·m is shown in Fig. 18(b). For a fair of comparison, the efficiency lookup table method [13] is tested at the same condition, and the results are shown in Fig. 18(a). It can be seen that the tracking process in the *d*-axis current will be quite obvious, whereas there is almost no significant tracking process in the *q*-axis current for both the proposed method and the lookup

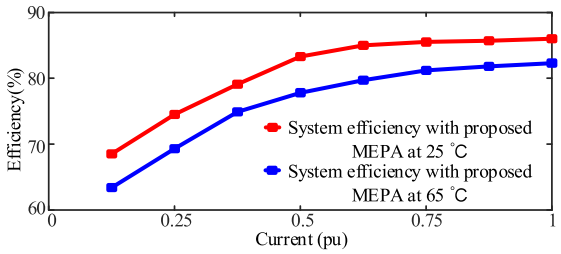

Fig. 19. System efficiency comparison under different current load at temperature 25 °C and 65 °C.

table method. It can be concluded that the proposed method exhibits faster dynamic performance, and operates stably after adjustment. The convergence time of the current angle after the load torque change with the proposed method is shorter than that of using the lookup table method [13]. It is proved that the proposed method has better dynamic performance than the previous method reported in [13].

F. MEPA Tracking Operation Temperature Change Experiment

In order to verify that the proposed method can be used under different temperature conditions, the IPMSM is operated under the rated load for 30 min to heat the IPMSM to 65 °C. A special test about system efficiency is conducted at 1000 r/min under different loads, as shown in Fig. 19, for 25 °C and 65 °C, respectively.

In the end, the effectiveness of the proposed VSI method for searching the MEPA current angle is verified under various speeds and loads. It can be concluded that the system efficiency is significantly improved with the proposed algorithm under high speed and lower current operation conditions. For example, the efficiency with MEPA angle is 74.5%, and the efficiency with MTPA angle is 70.3% at the speed of 1000 r/min and 0.25 p.u. current. While, the efficiency increases from 85.6% to 86% with the MEPA angle to replace the MTPA angle at 1000 r/min and 2.7 A rated current. The efficiency improvement effect is the minimum under low speed and large load current operation conditions. The current angle error is less than 1° between the calculated angle and real angle, which verifies the effectiveness of the proposed method for tracking the MEPA angle. The small difference is due to the neglecting of the PM eddy current loss and other high-order harmonic iron losses. The proposed MEPA algorithm has been proved to be able to improve IPMSM drive system efficiency under various working condition.

V. Conclusion

A VHFSI-based method searching for the optimal MEPA current angle of the IPMSM drive system (electrical machine and inverter) is proposed in this article. Under the MEPA control, the current angle could be derived from the virtual efficiency model and updated online in each control period. It has a good feature that the VSI would not cause adverse loss and torque ripple increase. The effectiveness of the proposed VHFSI control method is demonstrated with extensive experiments under various operation conditions. Compared with existing methods for MEPA tracking, the proposed method shows a good searching accuracy and dynamic performance with simple implementation. Besides, in real application, such as high power electric vehicle and train, it also can be employed for the online searching of optimal operation efficiency point. Meanwhile, the proposed method is parameter independent to machine inductance and flux linkage variations. More importantly, the proposed method works below the base speed (in the constant torque region) and the consideration of the voltage limitation and working in over-modulation region will, therefore, be the priority of future researches.

References

[1] X. Chen, J. Wang, B. Sen, P. Lazari, and T. Sun, "A high-fidelity and computationally efficient model for interior permanent-magnet machines considering the magnetic saturation, spatial harmonics, and iron loss effect," *IEEE Trans. Ind. Electron.*, vol. 62, no. 7, pp. 4044–4055, Jul. 2015.

[2] D. Wang, J. Li, R. Qu, and W. Kong, "Adaptive second-order sliding-mode observer for PMSM sensorless control considering VSI nonlinearity," *IEEE Trans. Power. Electron.*, vol. 33, no. 10, pp. 8994–9004, Oct. 2018.

[3] A. V. Sant, V. Khadkikar, W. Xiao, and H. H. Zeineldin, "Four-axis vector-controlled dual-rotor PMSM for plug-in electricvehicles," *IEEE Trans. Ind. Electron.*, vol. 62, no. 5, pp. 3202–3212, Jul. 2015.

[4] H. Liu and J. Lee, "Optimum design of an IE4 line-start synchronous reluctance motor considering manufacturing process loss effect," *IEEE Trans. Ind. Electron.*, vol. 65, no. 4, pp. 3104–3114, Apr. 2018.

[5] A. T. D. Almeida, F. J. T. E. Ferreira, and A. Q. Duarte, "Technical and economical considerations on super high-efficiency three-phase motors," *IEEE Trans. Ind. Appl.*, vol. 50, no. 2, pp. 1274–1285, Mar./Apr. 2014.

[6] H. Ge, Y. Miao, B. Bilgin, B. Nahid-Mobarakeh, and A. Emadi, "Speed range extended maximum torque per ampere control for PM drives considering inverter and motor nonlinearities," *IEEE Trans. Power. Electron.*, vol. 24, no. 4, pp. 1071–1082, Apr. 2009.

[7] A. Consoli, G. Scarcella, G. Scelba, and A. Testa, "Steady-state and transient operation of IPMSMs under maximum-torque-per-ampere control," *IEEE Trans. Ind. Appl.*, vol. 46, no. 1, pp. 121–129, Jan. 2010.

[8] M. Cao, J. Egashira, and K. Kaneko, "High efficiency control of IPMSM for electric motorcycles," in *Proc. IEEE 6th Int. Power Electron. Motion Control Conf.*, 2009, pp. 1893–1897.

[9] Y. A. R. I. Mohamed and T. K. Lee, "Adaptive self-tuning MTPA vector controller for IPMSM drive system," *IEEE Trans. Energy Convers.*, vol. 21, no. 3, pp. 636–644, Sep. 2006.

[10] G. Liu, J. Wang, W. Zhao, and Q. Chen, " A novel MTPA control strategy for IPMSM drives by space vector signal injection," *IEEE Trans. Ind. Electron.*, vol. 64, no. 12, pp. 9243–9252, Dec. 2017.

[11] C. Lai, G. Feng, K. Mukherjee, J. Tjong, and N. C. Kar, "Maximum torque per ampere control for IPMSM using gradient descent algorithm based on measured speed harmonics," *IEEE Trans. Ind. Informat.*, vol. 14, no. 4, pp. 1424–1435, Apr. 2018.

[12] J. Lee, K. Nam, S. Choi, and S. Kwon, "Loss-minimizing control of PMSM with the use of polynomial approximations," *IEEE Trans. Power Electron.*, vol. 24, no. 4, pp. 1071–1082, Apr. 2009.

[13] R. Ni, D. Xu, G. Wang, L. Ding, G. Zhang, and L. Qu, "Maximum efficiency per ampere control of permanent-magnet synchronous machines," *IEEE Trans. Ind. Electron.*, vol. 62, no. 4, pp. 2135–2143, Apr. 2015.

[14] D. Hu, W. Xu, R. Dian, Y. Liu, and J. Zhu, "Loss minimization control of linear induction motor drive for linear metros," *IEEE Trans. Ind. Electron.*, vol. 65, no. 9, pp. 6870–680, Sep. 2018.

[15] M. C. D. Piazza and M. Pucci, "Induction-machines-based wind generators with neural maximum power point tracking and minimum losses techniques," *IEEE Trans. Ind. Electron.*, vol. 63, no. 2, pp. 944–955, Feb. 2016.

[16] C. Mademlis, I. Kioskeridis, and N. Margaris, "Optimal efficiency control strategy for interior permanent magnet synchronous motor drives," *IEEE Trans. Energy Convers.*, vol. 19, no. 4, pp. 715–723, Dec. 2004.

[17] F. Fernandez-Bernal, A. Garcia-Cerrada, and R. Faure, "Model-based loss minimization for DC and AC vector-controlled motors including core saturation," *IEEE Trans. Ind. Appl.*, vol. 36, no. 3, pp. 755–763, Mar./Jun. 2000.

[18] M. N. Uddin and J. Khastoo, "Fuzzy logic–based efficiency optimization and high dynamic performance of IPMSM drive system in both transient and steady–state conditions," *IEEE Trans. Ind. Appl.*, vol. 50, no. 6, pp. 4251–4259, Nov./Dec. 2014.

[19] S. Vaez, V. I. John, and M. A. Rahman, "An on–line loss minimization controller for interior permanent magnet motor drives," *IEEE Trans. Energy Convers.*, vol. 14, no. 4, pp. 1435–1440, Dec. 1999.
[20] Y. Jeong, S. Sul, S. Hiti, and K. M. Rahman, "Online minimum-copper-loss control of an interior permanent-magnet synchronous machine for automotive applications," *IEEE Trans. Ind. Appl.*, vol. 42, no. 5, pp. 1222–1229, Sep./Oct. 2006.
[21] M. N. Uddin and S. W. Nam, "New online loss-minimization-based control of an induction motor drive," *IEEE Trans. Energy Convers.*, vol. 23, no. 2, pp. 926–933, Mar. 2008.
[22] A. A. C. Rebolledo and M. A. Valenzuela, "Expected savings using loss-minimizing flux on IM drives—Part I: Optimum flux and power savings for minimum losses," *IEEE Trans. Ind. Appl.*, vol. 51, no. 2, pp. 1408–1416, Mar./Apr. 2015.
[23] S. Sridharan and P. T. Krein, "Minimization of system-level losses in VSI-based induction motor drives: Offline strategies," *IEEE Trans. Ind. Appl.*, vol. 53, no. 2, pp. 1096–1105, Mar./Apr. 2017.
[24] A. T. Alexandidis, G. C. Konstantopoulos, and Q. Zhong, "Advanced integrated modeling and analysis for adjustable speed drives of induction motors operating with minimum losses," *IEEE Trans. Energy Convers.*, vol. 30, no. 3, pp. 1237–1246, Sep. 2015.
[25] A. M. Bazzi and P. T. Krein, "Review of methods for real–time loss minimization in induction machines," *IEEE Trans. Ind. Appl.*, vol. 46, no. 6, pp. 2319–2328, Nov./Dec. 2010.
[26] J. Wang *et al.*, "An accurate virtual signal injection control of MTPA for an IPMSM With fast dynamic response," *IEEE Trans. Power Electron.*, vol. 33, no. 9, pp. 7916–7926, Sep. 2018.
[27] T. Sun, J. Wang, and X. Chen, "Maximum torque per ampere (MTPA) control for interior permanent magnet synchronous machine drives based on virtual signal injection," *IEEE Trans. Power Electron.*, vol. 30, no. 9, pp. 5036–5046, Sep. 2015.
[28] T. Sun, M. Koc, and J. Wang, "MTPA control of IPMSM drives based on virtual signal injection considering machine parameter variations," *IEEE Trans. Ind. Electron.*, vol. 65, no. 8, pp. 6089–6099, Aug. 2018.
[29] Q. Tang, A. Shen, P. Luo, W. Li, and X. He, "IPMSMs sensorless MTPA control based on virtual q-axis inductance by using virtual high frequency signal injection," *IEEE Trans. Ind. Electron.*, vol. 67, no. 1, pp. 136–146, Jan. 2020.
[30] G. Wang, H. Zhou, N. Zhao, C. Rui, and D. Xu, "Sensorless control of IPMSM drives using a pseudo-random phase-switching fixed-frequency signal injection scheme," *IEEE Trans. Ind. Electron.*, vol. 65, no. 10, pp. 7660–7671, Oct. 2018.
[31] M. Schweizer, T. Friedli, and J. W. Kolar, "Comparative evaluation of advanced three–phase three–level inverter/converter topologies against two–level systems," *IEEE Trans. Ind. Electron.*, vol. 60, no. 12, pp. 5515–5527, Dec. 2013.
[32] M. Saur, W. Xu, B. Piepenbrier, and R. D. Lorenz, "Implementation and evaluation of inverter loss modeling as part of DB–DTFC for loss minimization each switching period," in *Proc. 16th Eur. Conf. Power Electron. Appl.*, 2014, pp. 1–10.

Mengdi Li received the M.S. degree in electrical engineering in 2017 from Hunan University, Changsha, China, where he is currently working toward the Ph.D. degree in power electronics and electrical drive at the College of Electrical and Information Engineering.

His current research interest focuses on advanced control of permanent magnet synchronous motor drive.

Sheng Huang received the M.S. and Ph.D. degrees from the College of Electrical and Information Engineering, Hunan University, Changsha, China, in 2012 and 2016, respectively.

He is currently a Postdoc with the Center for Electric Power and Energy, Department of Electrical Engineering, Technical University of Denmark, Lyngby, Denmark. His research interests include renewable energy generation, modeling and integration study of wind power, control of energy storage system, and voltage control.

Xuan Wu was born in Hunan, China, in 1983. He received the M.S. and Ph.D. degrees in automation from the College of Electrical and Information Engineering, Hunan University, Changsha, China, in 2011 and 2016, respectively.

From 2016 to 2019, he was a Postdoc with the College of Electrical and Information Engineering, Hunan University, where he is currently an Associate Professor. His research interests include permanent magnet synchronous motor drives and position sensorless control of ac motors.

Kan Liu (M'14–SM'17) received the B.Eng. and Ph.D. degrees in automation from the Hunan University, Changsha, China, in 2005 and 2011, respectively, and the Ph.D. degree in electronic and electrical engineering from The University of Sheffield, Sheffield, U.K., in 2013.

From 2013 to 2016, he was a Research Associate with the Department of Electronic and Electrical Engineering, The University of Sheffield. From 2016 to 2017, he was a Lecturer with the Control Systems Group, Loughborough University.

He is currently a Professor of electro-mechanical engineering with the Hunan University. His research interests include parameters estimation and sensorless control of permanent magnet synchronous machine drives and compensation of inverter nonlinearity, for applications ranging from automotive engineering to servo system.

Prof. Liu serves as an Associate Editor for the IEEE ACCESS, and also a Guest Editor/Associate Editor for the *Journal of Control Science and Engineering*, the *International Journal of Rotating Machinery*, and the *CES Transactions on Electrical Machines and Systems*. He is also the Acting Director of the Engineering Research Center, Ministry of Education on Automotive Electronics and Control Technology.

Xiaoyan Peng received the B.S. and M.S. degrees in mechanical engineering, and the Ph.D. degree in automatic control from Hunan University, Changsha, China, in 1986, 1989, and 2013, respectively.

She is currently a Professor with the College of Mechanical and Vehicle Engineering, Hunan University. Her research interests include control of mechatronic systems and safety analysis of autonomous vehicles.

Ge Liang received the B.S degree in electrical engineering in 2018 from Hunan University, Changsha, China, where he is currently working toward the Ph.D. degree in power electronics and electrical drive with the College of Electrical and Information Engineering.

His current research interest focuses on advanced control of permanent magnet synchronous motor drive.